Investigating residual stress along the interface of Dissimilar Metal Welds (DMWs)

Conference Paper · August 2017

CITATIONS
0

READS
27

3 authors, including:

Alison O'Connor
University of Limerick
9 PUBLICATIONS **17** CITATIONS
SEE PROFILE

C.M. Davies
Imperial College London
178 PUBLICATIONS **3,133** CITATIONS
SEE PROFILE

Investigating residual stress along the interface of Dissimilar Metal Welds (DMWs)

A N O'Connor[1], K M Nikbin[1], C M Davies[1]
[1]Mechanical Engineering, Imperial College London, London SW7 2AZ, United Kingdom

ABSTRACT: Dissimilar Metal Welds (DMWs) are used in many industries to increase the service life of components in corrosive environments. Structural integrity assessments of these components are complicated due to the changes in microstructure and difficulties in estimating defect location and size. The interaction between primary and secondary stresses on crack driving force (CDF) is not well understood, particularly at the interface between materials, leading to structural integrity assessments that are overly conservative. This work considers defects orientated close to the interface of two materials. The materials investigated are nuclear grade ferritic steel (A508) clad welded with an austenitic stainless steel comprised of one layer 308 and two layers 309L. The original clad weld was subjected to Electron Beam (EB) welding to facilitate the manufacturing of compact tension (CT) specimens. A thermo-mechanical model of the EB welding process was used to predict residual stresses in compact tension specimens.

KEY WORDS: structural integrity, crack driving force, residual stress, dissimilar metal weld.

1 INTRODUCTION

1.1 Background

The commercial nuclear industry began expanding rapidly from the 1950's with the first commercial nuclear power plant (NPP) being connected to a Soviet power grid in 1954 [1]. In 2008 up to 350GWe (gigawatt electricity) accounting for 16% of the world's power was generated by 439 NPPs. It has been estimated that by 2030 the amount of electricity generated will increase to between 400-640GWe [2]. One of the major issues facing the nuclear industry today is the safe operation of aging RPVs. Many RPVs were designed to have an operational life of 40 years based on the fatigue usage calculations [2]. The International Atomic Energy Agency (IAEA) has stated that approximately 25% of the world's NPPs have been in operation for 30 years and about 70% for more than 20 years [3].

Structural integrity procedures for NPPs were redeveloped after two significant nuclear accidents – the Three Mile Island incident (1979) and the Chernobyl accident (1986) both of which have been well documented [1, 4-7]. The new structural integrity procedures were rigorous methodologies assessing the level of risk in a quantifiable manner and were generally resubmitted to government overseers every 10 years [8]. The process of reassessment, where operators submit a quantifiable measurement of reliability (a safety case) to the relevant overseeing body, is still active today. One of the benefits of the safety case methodology is that should the NPP be deemed fit-for-purpose (FFP) the operational life may be extended beyond that of the original design. In the UK the R6 code [9] specifically addresses the assessment of defects and has a major influence on whether a NPP is deemed to have sufficient structural integrity. The overall project aims to increase knowledge about the fracture toughness of dissimilar metal welds with a view to reducing conservatism for life assessment programmes. This report focusses on deriving residual stresses in fracture test specimens. Allowing for accurate crack driving forces (CDFs) to be assessed in complex specimens, reducing the amount of conservatism required in structural integrity assessments.

1.2 Aims and Objectives

The aim of this work is to derive a residual stress profile using FE analyses which is in good agreement with experimental results. This will be achieved using the following objectives:

- Create a weld simulation using weld process parameters
- Map stresses from the coupled structural model to a second structural model
  - Investigate the influence of mesh density on result
  - Investigate the influence of mesh structure on result
- Compare resulting residual stress profiles with experimental results

2 EXPERIMENTAL WORK

2.1 Received materials

A section of clad plate measuring 70×180×58.5mm was received from previous work [10, 11]. From the previous works it is understood that the clad layers were welded using an automatic TIG (tungsten inert gas) process.

To assess whether the orientation of the notch with respect to the clad weld significantly affects crack propagation specimens taken from this material were notched along the interface between the ferritic and austenitic materials. Given the orientation of the cladding to the ferritic material and the dimensions of the original plate (70×180×58.5mm) it was not possible to machine standard size CT specimens from the as received material. The as-received material was machined into smaller sections comprised of two sections of ferritic only material (35×160×20mm) and, two sections of combined ferritic and austenitic material (35×160×26mm). The cladding surfaces were machined to a flat surface finish.

A ferritic only section was tack welded to the combined ferritic/austenitic section, effectively sandwiching the cladding between the ferritic sections. Two components 'Block A' and 'Block B' were manufactured.

Subsequent to tack welding the components were fused together using electron beam (EB) laser welding. The travel speed of the beam was 400mm/min. The voltage was specified to be 150kV with a beam current of 30mA. The beam diameter was calculated to be approximately 2mm. The depth of penetration was estimated at 20mm. The components were welded on both sides ensuring full fusion at the weld root.

Once in the EB chamber one side of Block A was welded, followed by one side of Block B. The chamber was vented and the temperatures on the surfaces of both blocks were measured using a temperature probe. The blocks were then flipped upside down, the chamber was re-pressurised, and the second side of each block was welded. Again Block A was welded first, followed by Block B. On venting the chamber the surface temperature of each block was again measured. The final EB welds on Block B are shown in Figure 1.

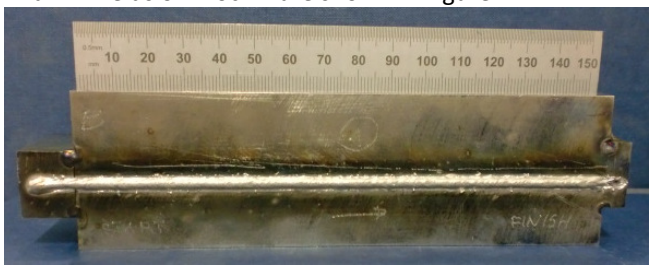

a)

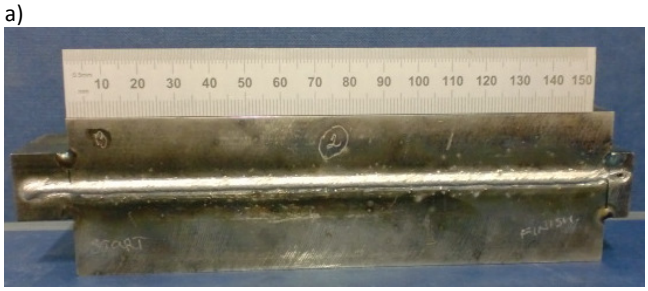

b)

Figure 1: EB welds for a) Block B, side 1, b) Block B, side 2

Post laser welding Block B was machined to remove the end blocks and weld caps. The original interface (i.e. the interface existing to the TIG weld, away from the EB weld) between the cladding and the ferritic steel was marked. CT specimens with notches orientated parallel to the original TIG weld interface were machined. The interface between the materials is not flat but undulated. Post-machining the notch tip was measured to be approximately 1.0-1.5mm from the clad weld interface. Machining was conducted using electro-discharge machining (EDM) process with a 0.25mm diameter wire. A total of six CT specimens measuring 37.5×36×15mm and three CTs measuring 37.5×36×3mm were machined from the component. Specimens were machined in batches of three beginning 10mm from the weld start position, with 12.5mm distance between each subsequent batch of specimens. Figure 2 shows the first batch (i.e. those closest to the weld start position) of CT specimens, including the variation in thickness and a magnified view of the notch position. As shown the notch tip is located in the austenitic material close to the original TIG weld.

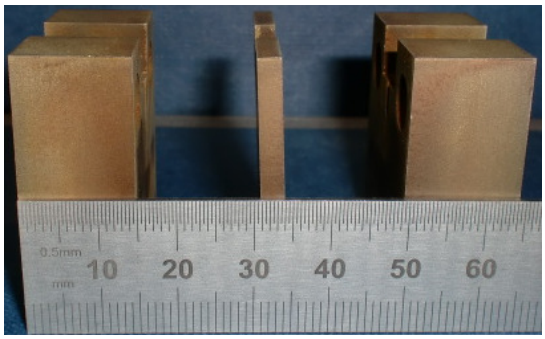

a)

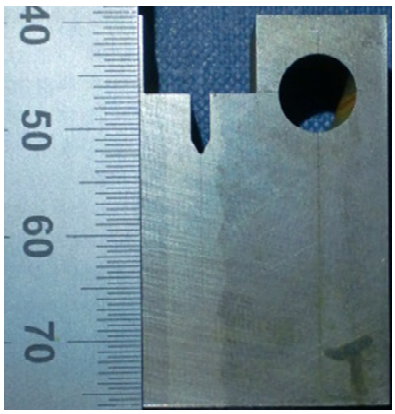

b)

Figure 2: a) First batch of three CT specimens, b) Magnified view of notching

2.2 Neutron Diffraction Measurements

Neutron diffraction measurements were made on the EB welded component Block A and on a CT specimen located at the weld start position of Block B, side 1. The measurements were taken using the instrument E3 at Helmholtz Zentrum Berlin (HZB). To ensure accurate residual strain measurements the reference lattice parameter, d_o, was determined using three individual cubic samples, each measuring 2×2×2mm^3, comprised of: ferritic material only, austenitic material only, and a combined ferrite and austenite material.

Due to the relative thickness of 'Block A' measurements were made transverse to the EB weld along the mid-weld mid-plane only. The majority of measurements were taken close to the EB weld and through the austenitic material. A total of 15 measurements (biased towards the weld region) were made. Locations close to the material boundary were measured twice, once for ferritic material and once for austenitic material as the composition of materials in these regions was not clear. Table 1 lists the measurement locations. To keep the count times reasonable a 2×10×2mm^3 gauge volume was utilised in the transverse and normal directions. A smaller gauge volume measuring 6×2×2mm^3 was utilised for the longitudinal measurements to increase the accuracy of the result.

Table 1: Location of neutron diffraction measurements on Block A

Measurement number	Distance from edge of sample (mm)	Material
1	5	Ferrite
2	15	Ferrite
3	20	Ferrite
4	25	Austenite
5	25	Ferrite
6	27	Austenite
7	27	Ferrite
8	30	Austenite
9	30	Ferrite
10	32	Austenite
11	32	Ferrite
12	35	Austenite
13	35	Ferrite
14	40	Ferrite
15	45	Ferrite

The CT specimens were relatively thin in comparison with the welded component therefore a gauge volume of 1×1×2mm^3 was utilised. A total of 12 measurements were taken in the mid-thickness of the specimens, starting from the crack tip continuing in increments of 2mm to the end of the sample, these are outlined in Table 2.

Table 2: Location of neutron diffraction measurements on Block A

Measurement number	Location from notch tip	Material
1	0	Austenite
2	2	Austenite
3	4	Austenite
4	6	Austenite
5	8	Austenite
6	10	Austenite
7	12	Austenite
8	14	Austenite
9	16	Austenite
10	18	Austenite
11	20	Austenite
12	22	Austenite

3 FINITE ELEMENT MODELLING

Finite element modelling (FEM) was conducted using commercial software Abaqus v6.14 from Dassault Systemes [12].

The geometry of the component was assumed to be identical to the machined sections prior to tack welding and laser welding. The component was assumed to be in a stress free condition prior to laser welding. Both the original clad welding and the tack welding processes were neglected from the analysis. The residual stresses due to the clad welding process were deemed likely to have been relieved close to a stress free state due to the machining process. The tack welding was neglected from the analysis under the assumption that the influence on residual stresses would be negligible in comparison to those present due to the laser welding process.

Temperature dependent material properties were taken from literature [11]. The density of both base and clad materials was assumed to be 7833 kg/m^3, the Poisson's ratio was assumed to be 0.3 irrespective of temperature. The heat transfer and structural models were identical to one another in terms of geometry, partitioning and materials properties. The models were partitioned so that material properties for both ferritic and austenitic sections could be applied to the relevant regions.

3.1 Heat Transfer Modelling

The heat flux was calculated using Equation 1, where η represents the efficiency of the welding process, V is the voltage, I is the current and v, the travel speed. The efficiency was assumed to be 1.00 (100%), the welding parameters used to calculate the heat flux as detailed earlier.

Abaqus requires the heat flux to have units associated with the volume of material to be heated. In the case of the 3D analysis this included the height, width and length of the weld beads. Each weld bead was assumed to have an equal height of 20mm (the depth of penetration), the length of the bead was known to be 160mm (i.e. the length of the component). The weld bead width was assumed to be 2.0mm (diameter of the laser).

$$Q = \frac{\eta V I}{(Area)v} \qquad \text{Equation 1}$$

The heat flux was calculated to be 7.03×10^8 W/m^3 per weld bead, assuming each bead takes 24 seconds to lay down. The heat transfer analysis was conducted using the block dump technique. The analysis followed the experimental procedure in terms of heating and cooling. The model was meshed using approximately 34,000 DC3D8 heat transfer elements.

Radiation conditions were applied to the relevant surfaces during the first and second cooling steps. Film and radiation conditions were applied during the third cooling step to simulate cooling outside the EB chamber. The radiation emissivity was assumed to be 0.75 while the film conditions were assumed to be 25W/m [11]. The final cooling step was applied until the block reached room temperature (20-25^{o}C). Cooling was assumed to occur at all surfaces except the one in contact with the EB chamber. The surface in contact with the EB chamber was assumed to be fully insulated (i.e. no cooling takes place).

3.2 Structural Modelling

The structural model calculated stresses from the nodal temperatures resulting from the heat transfer analysis. The model was identical to the heat transfer model in terms of geometry and applied material properties. The mesh was modified to use C3D20R structural elements but contained the same number of nodes and elements as the heat transfer model. Boundary conditions to constrain rigid body motion

were applied to corner nodes on one surface of the sample. All four corner nodes were constrained from moving in the z-direction (U3=0). One node was additionally constrained in both the x and y directions (U1=U2=U3=0), one node was additionally constrained in the x-direction (U1=U3=0). The applied boundary conditions are shown in Figure 3. The Von Mises stresses in Figure 3 are shown in Pascal units.

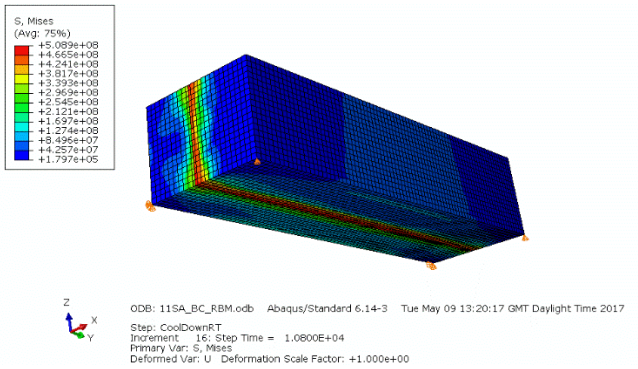

Figure 3: Boundary conditions applied to all structural models

As previously stated the purpose of this work is to investigate the estimated residual stresses in both the EB welded block and the CT specimens. Due to resource constraints it was not possible to model the geometry in sufficient detail, including the necessary partitioning and increased mesh density, to capture information on the individual CT specimens during the original structural analysis. To estimate the residual stresses in the CT specimens it was necessary to map the solution from the original model onto separate analyses that were partitioned accordingly.

Abaqus provides a number of methods to map solutions from one structural model to another. Two were investigated: the mapping of stresses using the predefined field method within Abaqus CAE software and, the mapping of stresses by modifying the input file to include the *MAP SOLUTION keyword. Table 3 lists the structural models assessed as part of this work. The predefined field method was found to be unsuitable when the mesh strategy was modified significantly in comparison to the original model and is therefore considered only suitable when discussing the original structural model (i.e. the model used to map nodal temperatures from the heat transfer model). MAP_1, MAP_2, and MAP_8 will not be discussed in the results section for the given reason.

Table 3: Mapped structural analyses

Name:	Mesh type	Number of elements	Element type	Mapping method
Original	Structured	34,560	C3D20R	Predefined field
MAP_1	Structured	34,560	C3D20R	Predefined field
MAP_2	Structured	250,240	C3D20R	Predefined field
MAP_3	Structured	34,560	C3D20R	*MAP SOLUTION
MAP_4	Structured	250,240	C3D20R	*MAP SOLUTION
MAP_5	Swept	42,408	C3D8R	*MAP SOLUTION
MAP_6	Swept	111,050	C3D8R	*MAP SOLUTION
MAP_7	Swept	34,560	C3D20R	*MAP SOLUTION
MAP_8	Swept	34,560	C3D20R	Predefined field
MAP_9	Swept	42,192	C3D20R	*MAP SOLUTION
MAP_10	Swept	112,350	C3D20R	*MAP SOLUTION

4 RESULTS AND DISCUSSION

4.1 Neutron Diffraction Results

4.1.1 Neutron Diffraction of Block A

The measured values of residual stress in the transverse, normal and longitudinal directions for EB welded Block A are plotted in Figure 4.

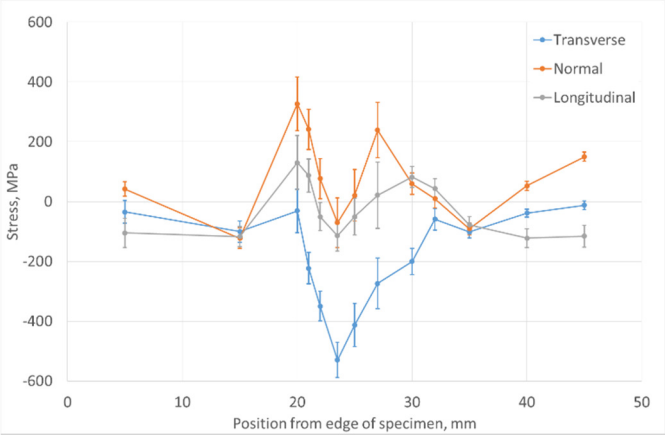

Figure 4: Measured residual stresses in the EB welded Block

From Figure 4 it can be seen that the maximum tensile stress is in the normal direction at the original cladding interface. A second peak tensile stress was found to exist at the EB weld location at the interface between the ferritic and austenitic materials. The longitudinal and transverse stresses also peak at the original clad weld interface but with magnitudes of stress that are lower than that found in the normal direction. The peak compressive stress was found to approximately 550MPa in the transverse direction in the austenitic material close to the EB weld boundary. Figure 4 clearly shows that stresses are at a maximum for all directions at the original clad weld interface. A second peak tensile stress occurs at the EB weld material interface for the normal direction and within 3-5mm of the EB weld interface for the longitudinal and transverse directions. The maximum compressive stresses for all three directions occurs approximately 2mm from the EB weld in the austenitic material.

4.1.2 *Neutron Diffraction of CT specimen*

The neutron diffraction results for the transverse, longitudinal and normal direction of the CT specimen located closest to the weld start position is shown in Figure 5. Stresses in the normal direction were assumed to be zero given the thickness of the samples and the gauge section utilised in the normal direction. As shown the transverse and longitudinal stresses are predicted to be in compression at the notch tip. The transverse stress measured as compressive in all locations except one, approximately 12mm from the notch tip where a tensile stress of 26MPa was found. The longitudinal stress is initially compressive but reaches a peak tensile force of approximately 100MPa within 5mm of the notch tip.

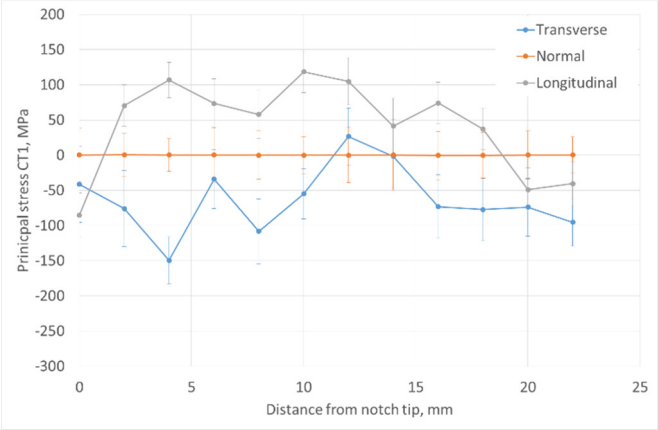

Figure 5: Measured longitudinal residual stresses in CT specimens from weld start (CT1), mid-weld (CT2) and weld stop (CT3) positions

4.2 *Finite Element Modelling Results*

4.2.1 *Heat Transfer Modelling*

The nodal temperatures were mapped from the heat transfer model to an identically meshed structural model using the predefined field function. The temperature profile of a specific node on both models is shown in Figure 6. As can be seen the temperature profiles are identical indicating that the nodal temperatures were transferred successfully.

It is interesting to note that the maximum temperature at the chosen node was estimated to be approximately 250 degrees Celsius (^{o}C). In fact the maximum temperature of the block during welding was measured to be 540^{o}C at a location corresponding to the location of this node at a similar stage of the analysis.

The predicted values of temperature imply that neither the ferritic nor austenitic materials reach the annealing or melt temperatures during EB welding. It should be noted however that this analysis is based on applying a heat flux to a relatively large area for a sustained period of time. In reality a moving heat source, such as a laser torch, would apply the same heat flux concentrated to a much smaller region for a relatively short time. The influence of assuming a block dump model adequately represents a moving heat source will be investigated in a later work.

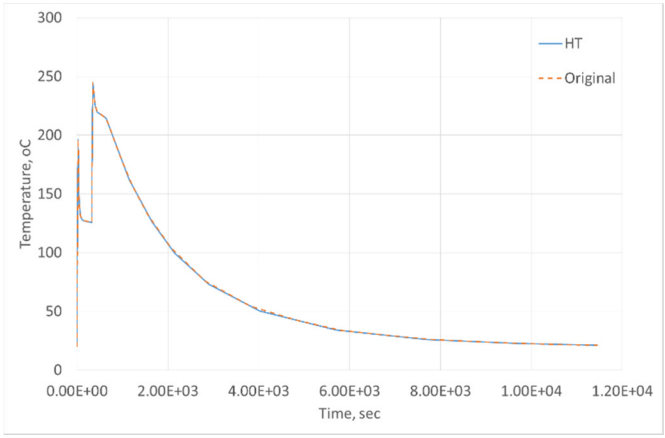

Figure 6: Nodal temperature versus time for identical node on heat transfer and original structural model

4.2.2 *Original Structural Model*

A path transverse to the weld, in the mid-thickness of the mid-plane of the specimen, analogous to the position of the experimental neutron diffraction measurements on Block A was used to estimate residual stress due to the EB welding process. The results are plotted in Figure 7 in comparison to the experimental data.

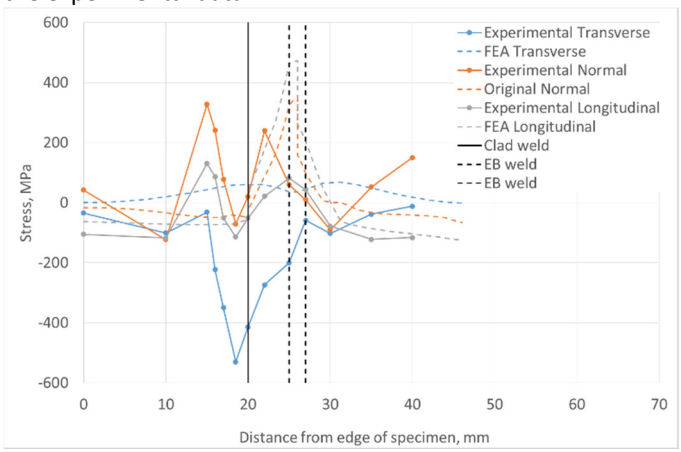

Figure 7: Original structural model estimated residual stresses in comparison to experimental data

As shown the FE simulation estimates the peak longitudinal (S22) and normal stresses (S33) to occur in the austenitic material in the region of the weld. Experimental data for these directions show that while a peak exists in the austenitic material it does not have a magnitude as large as that predicted by the FE model. The FE model fails to predict the double peak noted experimentally. This is attributed to the clad welding processes being neglected in the FE model. The experimentally measured transverse stress (S11) is shown to be compressive through the thickness of the component with significant changes in magnitude in the region of the weld. Conversely the FE model predicts a tensile stress with little change in magnitude.

4.2.3 *Mapping using *MAP SOLUTION keyword*

A comparison of the estimated transverse residual stress profile for simulations using the *MAP SOLUTION keyword is

shown in Figure 8. It can be seen that a good agreement in terms of both profile and magnitude of stress was noted for each subsequent simulations compared to the original structural model. There are slight differences in peak stress noted for MAP_5 and MAP_6 which used a different element type in comparison to the original structural analysis. MAP_5 and MAP_6 were conducted assuming a C3D8R element type while the original analysis used a C3D20R element. Computationally this requires mapping to less nodes than that which were contained in the original analysis, hence a less refined result is likely to be achieved. Comparing MAP_5 to MAP_6 shows that when the mesh density is increased the solution is more closely aligned to that predicted by the original structural model.

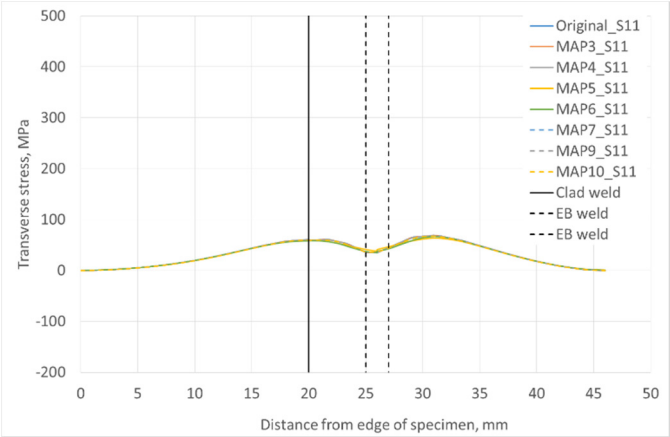

Figure 8: Comparison of transverse stresses for simulations using *MAP SOLUTION mapping method

The longitudinal and normal stresses are compared in Figure 9 and Figure 10 respectively. Again MAP_5 and MAP_6 are shown to have some variation in comparison to the original structural model but the remaining simulations are in good agreement with the original structural model.

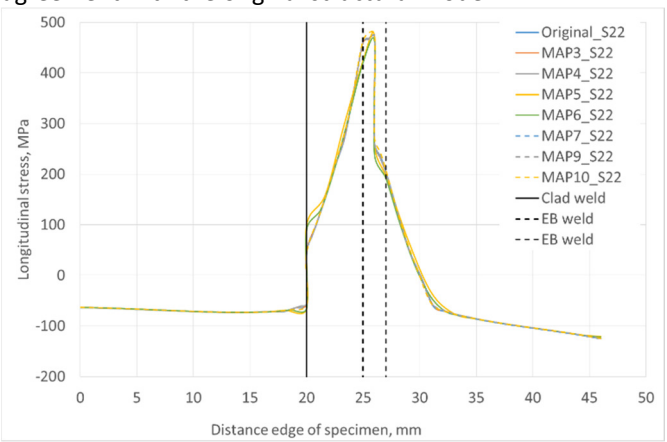

Figure 9: Comparison of longitudinal stresses for simulations using *MAP SOLUTION mapping method

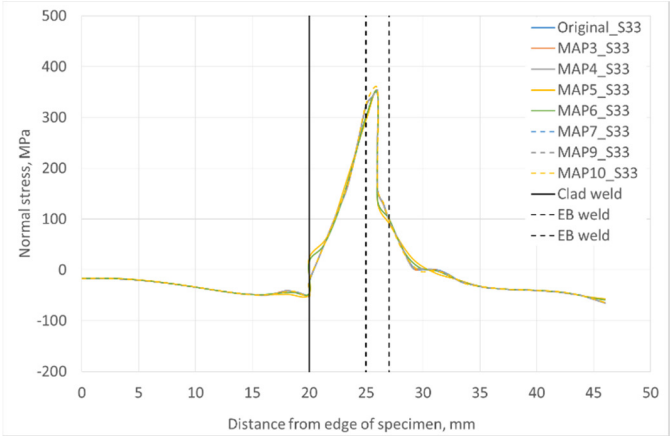

Figure 10: Comparison of normal stresses for simulations using *MAP SOLUTION mapping method

4.2.4 CT specimen FE results

The estimated residual stresses in the CT specimens is compared to those measured experimentally in Figure 11.

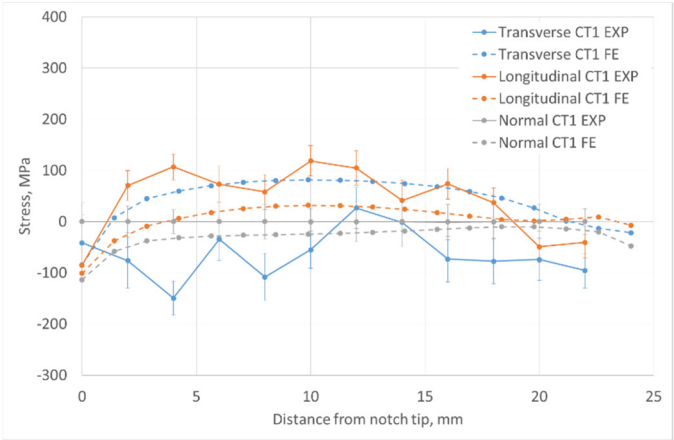

Figure 11: Comparison of experimental and FE stresses for CT1 (weld start position)

From Figure 11 it can be seen that the stresses estimated at the notch tip for CT1 in both the longitudinal direction and normal directions are a reasonable representation of those measured experimentally. The normal stress estimated using FE matches reasonably well with that measured experimentally except at the notch tip.

The measured transverse stress deviates significantly compared the predicted FE. Measured values clearly indicate that the transverse stress is, in the majority of locations, compressive. The single exception being a tensile stress of approximately 100MPa located 13mm from the notch tip. Conversely the predicted values of transverse stress indicate the majority of positions to be tensile with exceptions being the notch tip, and measurement locations occurring after 22mm from the notch tip.

The measured and predicted longitudinal stresses follow similar profiles over the length of measurement positions. However, it can be clearly seen that the predicted FE stresses fail to reach the peak magnitudes measured experimentally. Experimental results show peak tensile stress of approximately 100MPa exist 4mm from the notch tip,

predicted values at this location reach a peak of approximately 6MPa only. A similar deviation in result occurs 14mm from the notch tip, again a measured longitudinal stress of 100MPa was found whereas FE modelling predicted a longitudinal stress of approximately 30MPa. These deviations fall outside of the measured error limits.

All values of stress predicted using FE modelling show relatively smooth changes over the measured positions whilst experimental values show significant changes in profile over relatively small measurement changes. This is most notable at measurement positions between 12-16mm from the notch tip. In this location FE predicted values do not change significantly and a smooth trend is noted. Conversely measured values show that a peak tensile stress in the transverse and longitudinal directions occurs at 12mm from the notch tip.

While geometrical differences between the experimental and theoretical approaches may account for some of the deviations noted above it does not account for the significant changes in trend noted experimentally. It is considered likely that these changes in trend over the position of measurement are due to residual stresses attributed to the original clad weld which were neglected from the FE analysis. This would indicate that significant values of stress exist in the original components prior to EB welding.

5 CONCLUSIONS

- The block dump method for heat transfer analysis results in temperatures that are significantly lower than those expected to occur in reality. The influence of the result, in terms of the application of materials properties to the model, cannot be quantified in this work but is likely to significantly affect the reported residual stresses.
- The assumption that the clad welding process could be neglected from the analysis has been shown to be inaccurate for both the welded block ('Block A') and the CT specimen.
- Two methods of mapping stresses were investigated. The predefined field method was shown to be inaccurate in cases were the mesh differed substantially in comparison to the original mesh. The *MAP SOLUTION method is shown to accurately map the stress field even when the mesh was significantly different to that used originally. It should be noted however that the type of element chosen clearly influences the result and it is therefore recommended that elements used in the mapped analyses includes, at a minimum, the same number of integration points used in the original mapping process.
- The predicted values of residual stress in CT specimens were shown to deviate significantly from experimentally measured values. Significant changes stress profile along the measurement positions was shown to exist experimentally, these trends were not reflected with FE analysis techniques.

REFERENCES

[1] J. Chater, A history of nuclear power, in: Nuclear Exchange, 2005.

[2] International Atomic Energy Agency (IAEA), Integrity of reactor pressure vessels in nuclear power plants: assessment of irradiation embrittlement effects in reactor pressure vessel steels, in: I.A.E.A. (IAEA) (Ed.) IAEA Nuclear Energy Series, International Atomic Energy Agency (IAEA), Vienna, 2009.

[3] International Atomic Energy Agency (IAEA), Ageing management for nuclear power plants: international generic ageing lessons learned (IGALL), in: Safety reports series, International Atomic Energy Agency (IAEA), Vienna, 2015.

[4] M.W.D. Cooper, Atomic scale simulation of irradiated nuclear fuel, in: Materials Science and Engineering, Imperial College London, Imperial College London, 2015, pp. 220.

[5] International Atomic Energy Agency (IAEA), Nuclear safety review 2014, in: Nuclear safety and security programme, International Atomic Energy Agency (IAEA), 2014.

[6] D.W. Rathod, S. Pandey, P.K. Singh, R. Prasad, Experimental analysis of dissimilar metal weld joint: Ferritic to austenitic stainless steel, Materials Science and Engineering: A, 639 (2015) 259-268.

[7] M.K. Rowinski, T.J. White, J. Zhao, Small and Medium sized Reactors (SMR): A review of technology, Renewable and Sustainable Energy Reviews, 44 (2015) 643-656.

[8] B. Tomkins, 1.09 - Structural Integrity Issues in the Nuclear Industry, in: I.M.O.R. Karihaloo (Ed.) Comprehensive Structural Integrity, Pergamon, Oxford, 2003, pp. 173-192.

[9] British Energy, R6: Revision 4, Amendment 6: Assessment of the integrity of structures containing defects, in, 2008.

[10] N. Naveed, Improving the spatial resolution of the contour method, in: Department of Engineering and Innovation, Open University, 2015.

[11] K. Serasli, Measurement and mapping of residual stresses in welded nuclear components, in: Mechanical Engineering, University of Bristol, 2014.

[12] Dassault Systemes Simulia Corp, Abaqus 6.14 Documentation, in, 2014.

ACKNOWLEDGEMENTS

We thank HZB for the allocation of neutron beamtime. This project has received funding from the European Union's Seventh Framework Programme for research, technological development and demonstration under the ***NMI3-II Grant number 283883***